IEEE Access
Multidisciplinary ⋮ Rapid Review ⋮ Open Access Journal

Received September 22, 2021, accepted October 12, 2021, date of publication October 15, 2021, date of current version October 27, 2021.

Digital Object Identifier 10.1109/ACCESS.2021.3120697

An Accurate Near-Field Focusing of Array Antenna Based on Near-Field Active Element Pattern and Infinitesimal Dipole Modeling

SUNG JUN YANG[1,2] **AND YOUNG DAM KIM**[3]

[1]Foundation for Research on Information Technologies in Society (IT'IS), 8004 Zürich, Switzerland
[2]Swiss Federal Institute of Technology (ETH) Zürich, 8092 Zürich, Switzerland
[3]Department of Electronics Engineering, Chungnam National University, Daejeon 34134, South Korea

Corresponding author: Young Dam Kim (youngdamkim@cnu.ac.kr)

This work was supported in part by the Basic Science Research Program through the National Research Foundation of Korea (NRF) funded by the Ministry of Education under Grant 2020R1A6A3A03038818, and in part by the Research Fund of Chungnam National University.

ABSTRACT There are mainly three issues for Near-Field Focusing (NFF) using an antenna array. First, it is required to know the distribution of the near electric field in 3D space for each antenna element. In general, a huge amount of data is required to express the near-field for each antenna element in a 3D space with high resolution. Second, in the trade-off relationship between efficiency and accuracy for NFF, we require to solve the optimization problem in which energy can be concentrated to the focal point. Solving optimization problems with near-field represented by huge amounts of data is very inefficient. Third, accurate NFF must be performed by reflecting the mutual coupling phenomenon between antennas. In this paper, there are three key ideas to overcome the issues in the NFF by improving both accuracy and efficiency. The first is the extraction of the infinitesimal dipole model (IDM) using the active element pattern. This makes it possible to obtain a mathematical model of the antenna that perfectly reflects the mutual coupling effect. The second is the acquisition of near-field data to an adaptive resolution grid with appropriate resolution using the extracted IDM. This re-radiated near-field data has both accuracy and efficiency by maintaining high resolution only for a focal point. The third is an efficient optimization method for a desired focal area with an arbitrary elliptical shape using convex optimization. Through simulations for the verification, 4 types of grids with various resolutions are used to the same NFF problem. The computational time of the proposed method in optimization for the NFF could be reduced to 8% with a similar focal shift compared to a type of the finest resolution. In addition, the accuracy of the electromagnetic analysis of the proposed method was verified through comparative verification with the MoM results.

INDEX TERMS Near-field focusing, array antenna, active element pattern, infinitesimal dipole modeling, convex optimization.

I. INTRODUCTION

Recently, near-field focusing (NFF) antennas have been actively applied to various fields [1]. The NFF systems can give a higher efficiency to communicate or transfer power in near-field at a specific point. Antennas for NFF are commonly designed as array antenna for the controlling phase of the radiated field. Since the density of the radiated field decreases sharply as distance from the antenna increases, the NFF antennas can be more useful to cases which high efficiency of the energy transfer is required [2]–[6], especially if the external noise or interference signals are strong. Far-field focusing which means maximizing the radiated field at a designated angle has the two degrees of freedom: the elevation and azimuth angle. As the applications of the far-field focusing, satellites, radars, base stations for mobile network adopt the far-field focusing techniques for the distant radiation. It is assumed that the radiated field is attenuated through the wave propagation with the same pattern in the angular domain. On the other hand, the three-dimensional variables in the NFF techniques are controlled because the angular pattern is not maintained in the near-field region. The NFF

The associate editor coordinating the review of this manuscript and approving it for publication was Hassan Tariq Chattha.

can be used in the probing and imaging of a specific small area [7]–[10]. In biomedical electronics, it can be applied to in-body imaging technologies to enhance resolution [11] or hyperthermia which is a type of medical treatment generating high heat on a specific point in human body [12]–[14]. Wireless power transfer [15]–[18] and fifth-generation communication systems also directly require the NFF technique for high- energy or large data transfer efficiency in three-dimensional areas. Studying on the NFF techniques is being more active in recent years according to their needs than ever before.

There are mainly three issues to assess the performance of an NFF technique. The first is the accuracy of the NFF, and it basically depends on the quality and quantity of the near-field data. The three-dimensional parameters of x, y and z axes should be adjusted to control the field in the near-field region. Additional consideration of the radial distance makes it technically more difficult to obtain near-field data. Uncertainty of the measured position can affect to reliability of the field data, and the resolution can be limited following to the probe control problems. That is, quality and quantity of the obtained near-field data depends on the performance of the measurement instruments or function of the numerical simulations.

The second aspect is the efficiency of the optimization methods. In sequence, the optimization methods are applied to synthesize the field pattern in the near-field region. The near-field pattern can be controlled by adjusting the excitation coefficients (amplitudes and phases) in order to make the electromagnetic (EM) fields of the antenna elements be constructive each other at a specific position called 'focal point', the near-field can be regarded as 'focused'. Diverse optimization algorithms such as the phase conjugate [6], [19]–[22], least square method [23], compressive sensing [24], [25], and convex optimization [25]–[27] have been verified that can be used to synthesize near-field for the various cases as well as far-field synthesis problems. For the accuracy of the optimizations in the NFF, it is required to adopt a properly defined optimization problem and the solver. A large number of the observation points of near-field can degrade computational efficiency to solve the optimization problems. That is, the near-field data should be extracted from an appropriate number of observation points. It can be regarded that there must be a trade-off between the number of observation points of the near-field and the computational efficiency of the optimization. The importance of the computational efficiency is more emphasized in the NFF than the far-field focusing because the near-field data has one more dimensional variable, and it makes the constraints for near-field control more complex as the one-dimension. The relatively high-complexity of problem can increase the computational time and difficulty in the solution convergence.

The third is the antenna mutual coupling effect. Moreover, as sources of the optimizations, a number of accurate near-field data should be extracted with reflecting the mutual coupling between the antenna elements. Otherwise, the resulting near-field distribution represents the error although the optimization is well conducted. The following error is typically observed in terms of focal shift: the difference between the designated focal point and the point where the field is actually focused. The focal shift is a significant parameter to assess the accuracy of NFF systems.

In this paper, there are three key ideas to overcome the difficulties in the NFF by improving both the accuracy and efficiency. First, the antenna is modeled using a kind of theoretical modeling called infinitesimal dipole modeling (IDM). Because the IDM has been actively studied in many antenna analysis fields, it has been verified through various papers that the IDM can be used to predict the near-field or the far-field [28]–[31], [34], and numerous studies have been conducted to improve its modeling accuracy and efficiency [35]–[37]. Second, the near-field active element pattern (NAEP) is introduced to apply the AEP method in the near-field region. Third, a novel method is suggested to determine the resolution of the extracted NAEP as adaptive to the region such as focusing area or other areas, in an efficient way. The proposed NFF approach has advantages in the accuracy and efficiency of NFF problems. Applying the active element pattern (AEP) method plays as a solution to reflect the mutual coupling between the antenna elements [32], [33]. Modeling antennas by IDM enabl to obtain the near-fields at any points by a simple equation. Therefore, there is no limit in the resolution of near-field data, and we can apply the adaptive resolution in dealing with the near-field data which has more dense observation points near the focal point. It can maximize the optimization efficiency with maintaining the high accuracy of the proposed NFF approach.

Fig. 1 shows the flow chart of the proposed NFF algorithm consisting of 5 steps.

1) It is assumed that far-field AEP with a fixed resolution is already known through simulation or measurement.
2) We model each antenna element using IDM [28]–[31] from the AEP of far-field.
3) The near-field at any points in the radiated region can be predicted through mathematical model and the given equations. At this time, the near-field radiation region is divided into a focal region and other regions. The focal region can be set to high resolution and other regions set to low resolution. This allows for efficient and accurate implementation of the proposed NFF algorithm.
4) The obtained near-field becomes NAEP with an adaptive resolution grid.
5) The predicted near-field data set is applied to formally define the NFF problem. An iterative convex optimization is applied which represents high utilization and accuracy for the near or far-field synthesis.

Section II describes the basics of the IDM used for the NFF antenna. Section III describes the near-field optimization process using convex optimization, which is a type of optimization algorithm, based on IDM. In Section IV, the proposed NFF simulation and analysis results for the 16 Yagi array antenna are shown. Moreover, the proposed NFF approach and to verify its accuracy in comparison with the

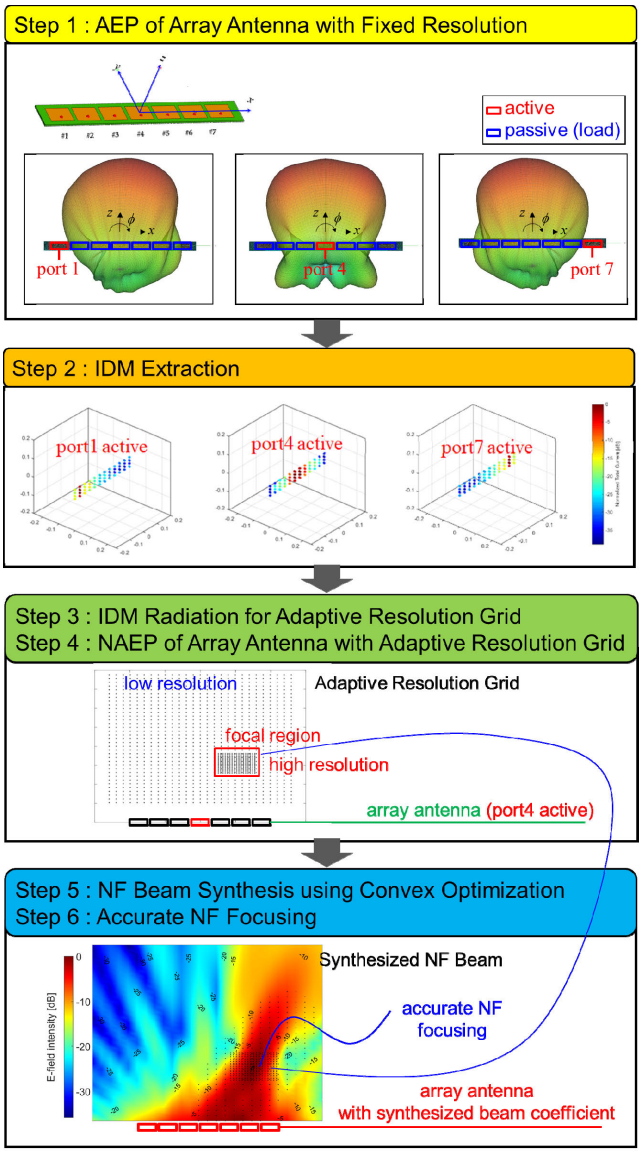

FIGURE 1. **Flow chart of the proposed NFF algorithm using 7-patch antenna array as an example.**

MoM, which is one of the full-wave EM analysis methods, using FEKO. FEKO is a commercial tool that supports numerical EM simulations. This paper is concluded in Section V.

II. RADIATION FORMULAS AND OPTIMIZATION OF IDM

Radiation field is the basis for model extraction using the IDM. In this section, the theoretical explanation of IDM radiation is first described, and then the proposed model extraction method is explained.

An antenna with a specific radiation field can be modeled as a distribution of IDs. An ID has a unique radiation field according to each of the seven variables: excitation amplitude (A_{ID}), phase (ψ_{ID}), orientation (θ_{ID}, ϕ_{ID}), and position (x_{ID}, y_{ID}, z_{ID}). The radiation field is expressed mathematically, and the general radiation field of the ID distribution is formulated as follows [1]:

$$\mathbf{E}_n(\mathbf{r}) = \sum_{n=1}^{N_{ID}} w_n^{ID} \frac{1}{j4\pi\omega\varepsilon_0} [k^2 ((\mathbf{n}_n \times \mathbf{p}_n) \times \mathbf{n}_n) \frac{e^{-jkr_n}}{r_n} + (3\mathbf{n}_n (\mathbf{n}_n \cdot \mathbf{p}_n) - \mathbf{p}_n) \left(\frac{jk}{r_n^2} + \frac{1}{r_n^3}\right) e^{-jkr_n}] \quad (1)$$

where $\mathbf{E}(\mathbf{r})$ is the electric field radiated by the n IDs at an observation point $\mathbf{r}$. ω is angular frequency of the field and ε_0 is permittivity in the free space. k is the wavenumber. $\mathbf{n}_n$ and $\mathbf{p}_n$ are the unit vector from n^{th} ID to the observation point and the dipole moment of n^{th} ID. r_n is the distance between ID and the observation point. $\hat{\mathbf{r}}$ is the unit vector to the observation point and w_n^{ID} is the weighting coefficient of the n^{th} ID ($=A_{\mathrm{ID}} \times \exp(j\psi_{\mathrm{ID}})$). 1 j is square root of -1. The equation for the far-field of an ID can be obtained by reformulating (1) by getting rid of the second term as follows through a far-field approximation, which $1/r_n \gg 1/\mathrm{r}_n^2, 1/\mathrm{r}_n^3$.

In this study, the position and the direction of the ID are determined using the triangularly segmented computer-aided design (CAD) model of the modeled antenna to obtain the ID model with the highest efficiency [35], [36]. The triangular mesh, which is the most common segmentation model, is used for the MoM. Each ID can theoretically be regarded as a point current source. Therefore, it is possible that the higher the modeling accuracy is, the more similarity the ID distribution has to the actual current distribution. The position of each ID is the same as the center of each segment. Further, at each position, three IDs having the directions of x, y, and z axis are arranged. Therefore, when the number of segments is N_{seg}, the number of IDs, or the number of variables in the IDM problem $N_{\mathrm{ID}} = 3N_{\mathrm{seg}}$. In this study, the function of obtaining the triangular mesh from a CAD model built in the FEKO was used. When the ID distribution is formed by the segmented CAD model, (2) and (3) can be defined as the following linear problem:

$$\mathbf{E}_{\mathrm{pol}}^{\mathrm{near}}(\mathbf{r})\Big|_{\mathrm{pol}=x,y,z} = \sum_{n=1}^{3N_{\mathrm{seg}}} \mathbf{C}_{n,\mathrm{pol}}^{\mathrm{near}}(\mathbf{r}) \cdot w_n^{\mathrm{ID}}\Big|_{\mathrm{pol=x,y,z}}, \quad (2)$$

$$\mathbf{E}_{\mathrm{pol}}^{\mathrm{far}}(\mathbf{r})\Big|_{\mathrm{pol}=\theta,\phi} = \sum_{n=1}^{3N_{\mathrm{seg}}} \mathbf{C}_{n,\mathrm{pol}}^{\mathrm{far}}(\mathbf{r}) \cdot w_n^{\mathrm{ID}}\Big|_{\mathrm{pol}=\theta,\phi}, \quad (3)$$

where $\mathbf{E}_{\mathrm{pol}}^{\mathrm{near}}(\mathbf{r})$ and $\mathbf{E}_{\mathrm{pol}}^{\mathrm{far}}(\mathbf{r})$ are near and far-field radiated by the ID model for the specific polarization, respectively. $\mathbf{C}_{n,\mathrm{pol}}^{\mathrm{near}}$ and $\mathbf{C}_{n,\mathrm{pol}}^{\mathrm{far}}$ is the parameter to calculate the near and far-field of the ID model, respectively. $\mathbf{C}_{n,\mathrm{pol}}^{\mathrm{near}}$ and $\mathbf{C}_{n,\mathrm{pol}}^{\mathrm{far}}$ are constants because the positions and orientations of IDs are fixed in this scheme, and they can be obtained using (1) according to the observation point and polarization, and the expansion is omitted for the brevity.

The IDM refers to the process of finding an ID distribution with the same radiation pattern with the modeled antenna. In the proposed near-field synthesis approach, the ID models were obtained from the far-field pattern of the antenna. The far-field pattern can be measured or calculated by an

EM simulation. The far-fields of the antenna were calculated through the MoM supported by FEKO to verify the proposed method. When the obtained far-field data of the antenna are expressed in a matrix form for the angular domains, the optimization problem can be defined for the IDM using (3) as follows:

$$\mathbf{w}^{\mathrm{ID}} = \arg\min \left(\sum_{\theta,\phi} \left| \mathbf{E}_{\mathrm{pol}}^{\mathrm{far}}(\theta,\phi) - \mathbf{E}_{\mathrm{pol}}^{\mathrm{ANT}}(\theta,\phi) \right|^2 \right), \quad (4)$$

where θ and ϕ is the angular domains. $\mathbf{E}_{\mathrm{pol}}^{\mathrm{ANT}}(\mathbf{r})$ is the electric radiation field of the modeled antenna. The solution $\mathbf{w}^{\mathrm{ID}}$(column vector of variable w_n^{ID}) and the following ID model can be obtained efficiently by solving the least square problem in (4), which is expressed as a linear problem. In this study, the linear problem in (4) is solved using the LSQR function embedded in MATLAB [35].

III. NEAR-FIELD FOCUSING USING CONVEX OPTIMIZATION BASED ON NAEP-IDM

In this section, the procedure for obtaining the excitation coefficients of each ID to focus the synthesized near-field at the focal point from the far-field pattern of an array antenna is described. The descriptions follow to order of the steps of proposed NFF algorithm represented in the Introduction section and it is specified the explanation belongs to which step. The theoretical basis and features of each step are explained in detail according to the order of the proposed NFF approach.

A. OBTAINING NAEP ON ADAPTIVE RESOLUTION GRID USING IDM RADIATION

In the proposed NFF approach, the far-field AEP of the array antenna is used for the IDM extraction (*step 1*). The AEP is a technique that can directly reflect the mutual coupling effect between the elements of the array antenna [38]. If M antennas are arranged, M ID models for M AEPs should be extracted (*step 2*).

Using IDM radiation, near-field data can be obtained according to (2) using the IDM according to each far-field AEP. The re-radiated near-fields also reflect the mutual coupling effect between the antenna elements, and thus it can be called the near-field active element pattern (NAEP). The NAEP can be calculated in any area outside the antenna geometry. Any arbitrary antennas can be considered accurately for the proposed NFF approach even if the antenna elements have their own anisotropic patterns.

The number of equations in the optimization problem is proportional to the number of sampled points, and the computation time required to solve the optimization problem. Conversely, if the sampled points are too sparse, the desired near-field synthesis may not be achieved properly. The near-field region should be sampled with an appropriate density. Although there is no fixed rule to decide the density, the denser sampling in the focal region than the other region, the more accurate optimization for the NFF. In order to control the NAEPs efficiently, we propose an idea to adopt adaptive resolution as shown in *steps 3* and *4* in Fig. 1. The near-field radiation region is divided as the focal and non-focal region. After that, the near-field data is extracted in the focal region with high resolution and the non-focal region with low resolution (*step 3*). The near-field data at the sampled points are obtained by the simple calculation of the IDM in (2) without any additional measurements or EM numerical simulation (*step 4*).

With the adaptive resolution grid, the proposed approach can deal with dense and numerous sampled points efficiently. That is, adjusting the resolution according to the areas in the near-field region can improve the optimization efficiency and the accuracy simultaneously. Usually, as mentioned in the Introduction section, it is difficult to adjust the resolution by the measurements of near-field due to technical problems such as limitation of specification of the measurement instruments or the time consumption, and so on. However, it can be easily implemented in the proposed scheme because the near-field can be calculated by the equation (1) of the IDM method at any positions in the radiating region.

B. NEAR-FIELD FOCUSING USING CONVEX OPTIMIZATION

The near-field of the array antenna can be synthesized by superposition with weighting the excitation coefficients to each NAEP. This can be expressed by the following equation. For the antenna model, the excitation coefficients are multiplied to each ID according to the antenna elements.

$$\mathbf{E}_{\mathrm{pol}}^{\mathrm{near}}(\mathbf{r})\Big|_{\mathrm{pol}=x,y,z} = \sum_{m=1}^{M} w_m^{\mathrm{AEP}} E_{\mathrm{pol}}^{\mathrm{near},m}(\mathbf{r})\Big|_{\mathrm{pol}=x,y,z}. \quad (5)$$

The matrix on the left-hand side is the complex value of the electric field of the array antenna according to the position of the sampled near-field region for each x, y, and z polarization. $\mathbf{E}_{\mathrm{pol}}^{\mathrm{near},m}$ is the NAEP of the m^{th} port and w_m^{AEP} on the right-hand side is the excitation voltage applied to the port of each antenna element and is summed by multiplying the sampled NAEP corresponding to each antenna element. M is the number of antenna element of the modeled array antenna. In other words, this is the vector summation using the NAEP of the array antenna.

In the proposed NFF approach, the problem of increasing the intensity of the near-field at a specific focal point for with a relatively low value in the other region can be defined as following steps:

$$\mathbf{w} = [w_1^{\mathrm{AEP}},\ w_2^{\mathrm{AEP}},\ \cdots,\ w_M^{\mathrm{AEP}}]^T \quad (6\text{-}1)$$

$$\mathbf{E}_{\mathrm{pol}}^{\mathrm{near}}(\mathbf{r}) = \left[E_{\mathrm{pol}}^{\mathrm{near},1}(\mathbf{r}),\ \cdots,\ E_{\mathrm{pol}}^{\mathrm{near},M}(\mathbf{r}) \right]\Big|_{\mathrm{pol}=x,y,z}, \quad (6\text{-}2)$$

$$E_{\mathrm{pol}}^{\mathrm{near}}(\mathbf{r}) = \mathbf{E}_{\mathrm{pol}}^{\mathrm{near}}(\mathbf{r})\mathbf{w}\Big|_{\mathrm{pol}=x,y,z}, \quad (6\text{-}3)$$

where $\mathbf{w}$ is column vector in which elements are the weighting coefficients. $\mathbf{E}_{\mathrm{pol}}^{\mathrm{near}}(\mathbf{r})$ is row vector in which elements are field values of the NAEPs and $E_{\mathrm{pol}}^{\mathrm{near}}(\mathbf{r})$ is the

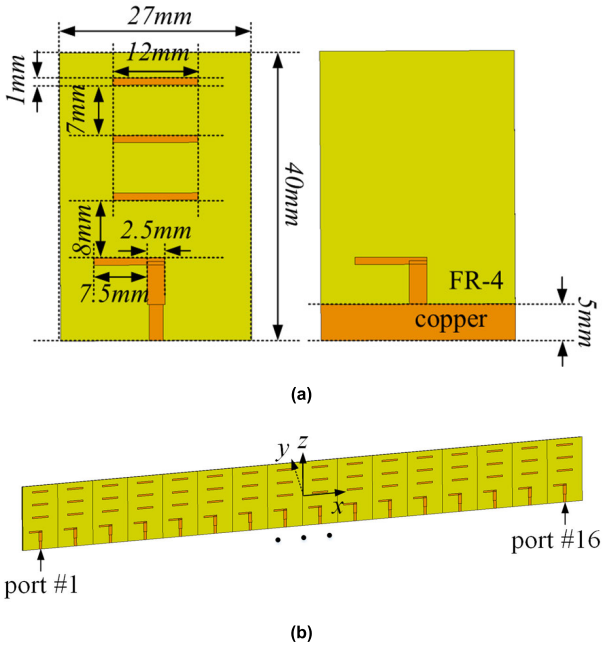

FIGURE 2. Designed CAD model of the 16 × 1 quasi-Yagi array antenna (a) single-Yagi antenna element designed at 5.8 GHz and (b) geometry of a 16 × 1 quasi-Yagi array antenna using the single-Yagi element.

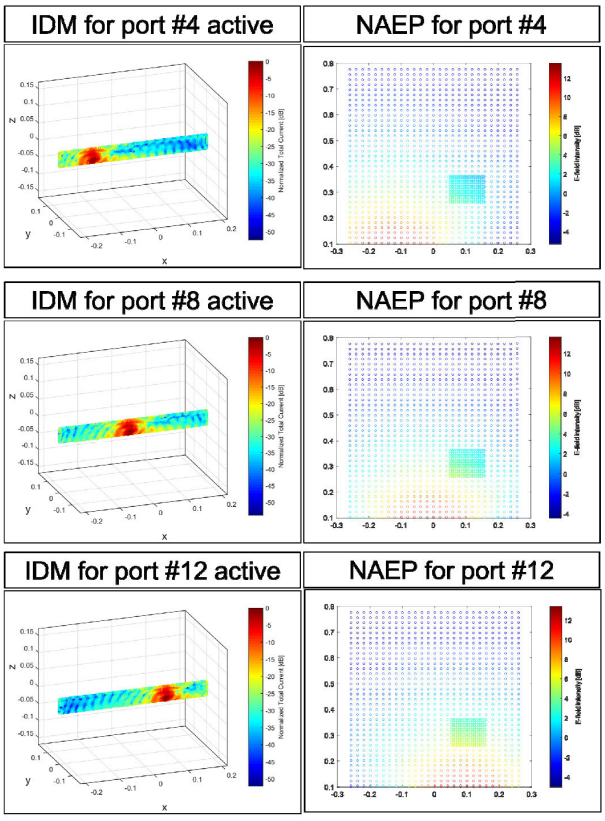

FIGURE 3. IDM results extracted using the simulated AEP for port 4, port 8 and port 12(left) and NAEP results obtained by re-radiating the corresponding IDM for near-field region on the adaptive resolution grid.

synthesized radiated near-field by the arrayed antenna elements at a position $\mathbf{r}$.

The intensity of the electric field for each case is defined as

$$\begin{aligned} \left|E_{\text{tot}}^{\text{near}}(\mathbf{r})\right|^2 &= \tilde{\mathbf{w}}^T Q_{\text{tot}}(\mathbf{r})\tilde{\mathbf{w}} \\ \left|E_{\text{pol}}^{\text{near}}(\mathbf{r})\right|^2 &= \tilde{\mathbf{w}}^T Q_{\text{pol}}(\mathbf{r})\tilde{\mathbf{w}}\Big|_{\text{pol}=x,y,z}, \end{aligned} \tag{7}$$

where

$$E_{tot}^{\text{near}}(\mathbf{r}) = \sqrt{E_x^{\text{near}}(\mathbf{r})^2 + E_y^{\text{near}}(\mathbf{r})^2 + E_z^{\text{near}}(\mathbf{r})^2}, \tag{8-1}$$

$$A_{\text{pol}}(\mathbf{r}) = \begin{bmatrix} \text{Re}\left(\mathbf{E}_{\text{pol}}^{\text{near}}(\mathbf{r})\right) & -\text{Im}\left(\mathbf{E}_{\text{pol}}^{\text{near}}(\mathbf{r})\right) \\ \text{Im}\left(\mathbf{E}_{\text{pol}}^{\text{near}}(\mathbf{r})\right) & \text{Re}\left(\mathbf{E}_{\text{pol}}^{\text{near}}(\mathbf{r})\right) \end{bmatrix}\Bigg|_{\text{pol}=x,y,z}, \tag{8-2}$$

$$Q_{\text{pol}}(\mathbf{r}) = A_{\text{pol}}^T A_{\text{pol}}\Big|_{\text{pol}=x,y,z}, \quad Q_{\text{tot}}(\mathbf{r}) = A_{\text{tot}}^T A_{\text{tot}}, \tag{8-3}$$

$$A_{\text{tot}}(\mathbf{r}) = \begin{bmatrix} A_x(\mathbf{r}) \\ A_y(\mathbf{r}) \\ A_z(\mathbf{r}) \end{bmatrix}, \tag{8-4}$$

$$\tilde{\mathbf{w}} = \begin{bmatrix} \text{Re}(\mathbf{w}) \\ \text{Im}(\mathbf{w}) \end{bmatrix}. \tag{8-5}$$

$\mathbf{W} = \tilde{\mathbf{w}}\tilde{\mathbf{w}}^T$ is rank-one positive semidefinite matrix, and $\mathbf{W}$ can be applied as a variable to be optimized for NFF problems as follows (in cases of considering total intensity of the radiated electric field) (*step 5*):

$$\begin{aligned} &\text{variable: } \mathbf{W}_k \\ &\text{minimize: } \text{Tr}\left(\mathbf{W}_{k-1} + \delta I\right)^{-1}\mathbf{W}_k \\ &\text{such that } \begin{cases} \text{Tr}\left(Q_{\text{tot}}(\mathbf{r}_{\text{center}})\mathbf{W}_k\right) \geq \text{c}_{\text{center}} \\ \text{Tr}\left(Q_{\text{tot}}(\mathbf{r}_{\text{in}})\mathbf{W}_k\right) \leq \text{Tr}\left(Q_{\text{tot}}(\mathbf{r}_{\text{center}})\mathbf{W}_k\right) \\ \text{Tr}\left(Q_{\text{tot}}(\mathbf{r}_{\text{out}})\mathbf{W}_k\right) \leq \text{c}_{\text{out}} \\ \mathbf{W}_k \text{ is positive semidefinite,} \quad \text{rank}(\mathbf{W}) = 1, \end{cases} \end{aligned} \tag{9}$$

where k is the number of iteration ($k = 1, 2, \ldots, N_{\text{iter}}$), and N_{iter} should be appropriately determined. $\delta > 0$ is a saturation constant which is smaller than elements of $\mathbf{W}_{k-1}$. I is a unit matrix. Initial value of $\mathbf{W}_k$, $\mathbf{W}_0$ is a unit matrix in this paper. More detailed explanations of the variables and parameters are represented in [39]–[41]. $\mathbf{r}_{\text{center}}$, $\mathbf{r}_{\text{in}}$, and $\mathbf{r}_{\text{out}}$ are position vector from origin to the focal point, positions inside the desired focal area, and positions outside the desired focal area, respectively. As the main-lobe for the NFF is usually observed as nearly elliptical, the focal area in (12) is a skewed-elliptical shape toward the focal point. The major axis of the ellipse is on a line from the center of an array antenna to the focal point. Based on the focal point, the half-power beam width (HPBW) in the range direction, which is perpendicular to the array antenna aperture, is referred to as the depth of focus (DoF). The HPBW in the azimuth direction, which is parallel to the antenna aperture, is referred to as the focal width (FW). The constants c_{center} and c_{out} are determined for the restriction of E-field intensity at $\mathbf{r}_{\text{center}}$ and $\mathbf{r}_{\text{out}}$, respectively. The optimization in (9) means that the excitation coefficients of the antenna elements are optimized under the constraints. Under the constraints, the synthesized

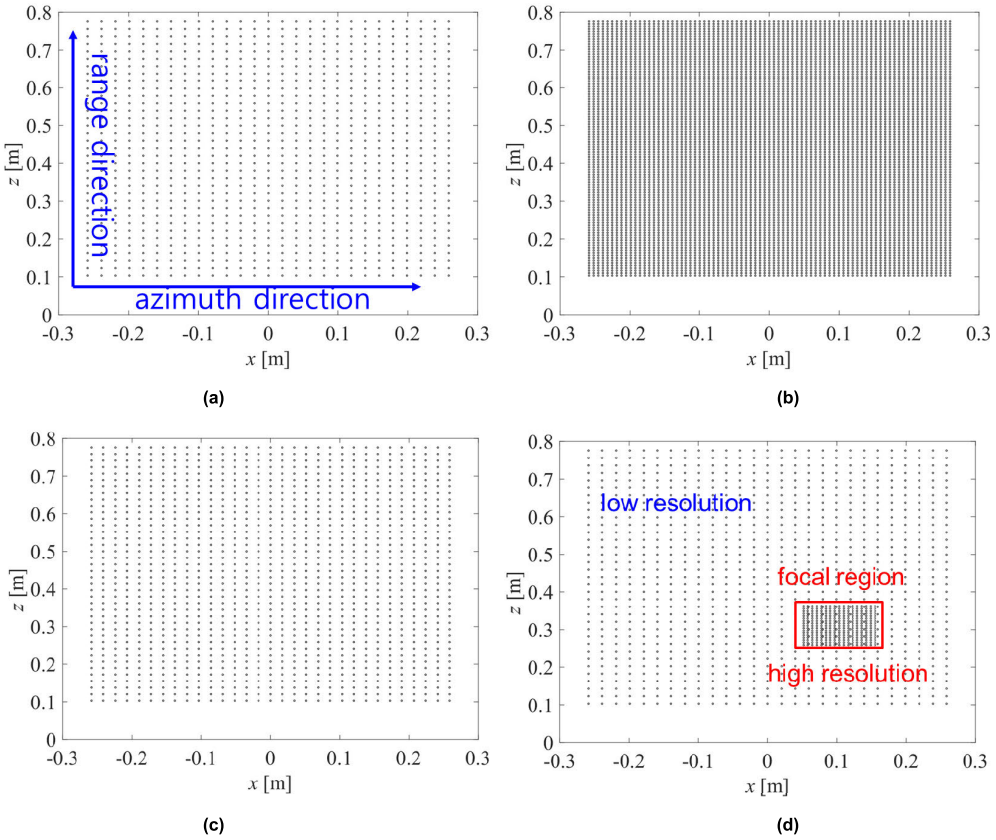

FIGURE 4. Four types of near-field grid for NAEP extraction (a) *resolution 1* (b) *resolution 2* (c) *resolution 3* and (d) *adaptive resolution*.

field intensity of the array antenna at the focal point should be larger than others. The field intensity should be in the focal area should be smaller than the focal point, therefore the focal point presents the maximized field intensity compared to the other points. Exterior to the focal area, the field intensity is suppressed as much as the predetermined value. To summarize the constraints, there should be a focal area with relatively larger field intensity than the exterior area, and the field should be maximized at the focal point in the focal area.

Equation (9) is a kind of relaxed problem of the convex optimization for the NFF let the rank($\mathbf{W}$) converge to 1 after the iterative optimization, and the relaxation method is called semidefinite relaxation (SDR) [39]–[41]. The convex optimization is one of the deterministic algorithms used to find solutions to problems through analytical approaches. The details of each condition are described in previous studies on the convex optimization [28]. It is well-known that various field patterns can be synthesized by varying the definition of the convex problem with SDR [39]–[41]. In this study, the MATLAB-based open source code CVX is used to implement the convex optimization [43].

After the optimization in (9), if rank($\mathbf{W}$) ≥ 1, $\mathbf{W}$ can be obtained using eigenvalue decomposition, $\mathbf{W} = \sigma u u^T$. σ is the largest eigenvalue of the $\mathbf{W}$, and u is corresponding eigenvector. $\tilde{\mathbf{w}} = \sqrt{\sigma} u$ and the weighting coefficients of the antenna elements can be obtained.

IV. NFF SIMULATION RESULTS AND ANALYSIS

We used the MoM, which is a numerical EM analysis technique supported by FEKO, to verify the proposed NFF approach as shown in Fig. 1. The proposed approach can be applied not only to uniform linear array antennas but also to all types of antennas which can be modeled by the IDM. In theory, with sufficient calculation time and memory, all types of antennas can be applied to the IDM. Following the previous studies, a number of types of antennas can be modeled by the IDM [28]–[31]. The simulation results are presented in the order of the proposed NFF approach shown in Fig. 1.

A. IDM OF 16 × 1 QUASI-YAGI ARRAY ANTENNA

For the simple verification of the proposed method, CAD models of 16 × 1 quasi-Yagi array antenna is used as shown in Fig. 2. The operation frequency is 5.8 GHz.

The far-field AEPs are obtained through the MoM calculation and applied to the AEP-IDM. The far-field AEPs obtained from the measurements or simulations and the far-field of the optimized ID model should have high agreement through the IDM procedure. The far-field data used in this study have amplitude and phase values for angular domains, and the theta and phi domains have 0°–180° and 0°–360° with 3° and 5° intervals, respectively. For the IDM to be used accurately, the far-field should be sampled dense in

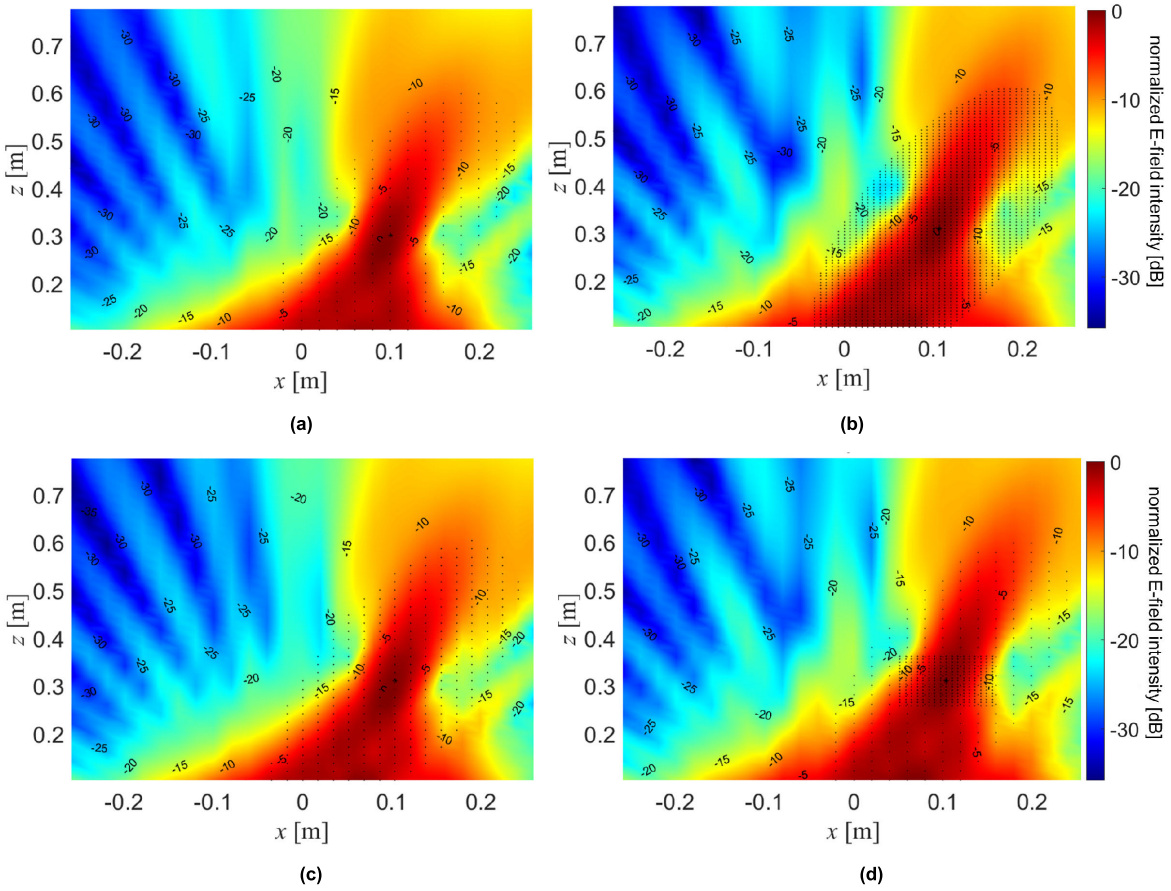

FIGURE 5. 2D NFF results using 4 type grids shown in Fig. 3 and the NFF simulation conditions summarized in table 1 (a) *resolution 1* (b) *resolution 2* (c) *resolution 3* and (d) *adaptive resolution*. Black dots are the observation points of the various resolutions in the predetermined focal area.

wide range of angles. If the far-field angular domain is sampled to an excessive number, the computational complexity increases, and obtaining an accurate ID model takes a long time.

For IDM extraction, the CAD model of the array Yagi antenna is segmented into a triangular mesh using the built-in function of FEKO and applied to the IDM. Depending on the geometry of the antenna, the segments are distributed in the x, y, and z domains within the xyz range of [−0.2160∼0.2160, 0∼0.001, and −0.02∼0.02] in meter. The length of the sides of the segments is approximately λ/20, and the array antenna is divided into 6,258 segments. λ is the wavelength for 5.8 GHz. Each ID model according to the 16 AEPs has $3 \times 6{,}258 = 18{,}774$ IDs, and each ID is placed at the center of each triangular segments. To quantify the accuracy of the IDM according to the optimization, the normalized root mean square errors between the far-fields obtained by the MoM and the far-fields optimized by the IDM are calculated. The resulting error values are about −92 dB for all the 16 ID models. The ID models are obtained highly similar to the far-field obtained by the MoM through an efficient optimization process. Fig. 3 shows the ID models corresponding to the extracted for active ports 4, 8, and 12. Finally, the 16 ID models can be obtained through the AEP-IDM. As the source data of optimization for the NFF, these are example of the IDM results and we can consider the ID models were obtained in a reasonable way according to the graphical profile of the ID distribution. The fact that high-amplitude currents are concentrated near the excited port is shown clearly in the Fig. 3. Moreover, the NAEPs also represent same trends as shown in the Fig. 3.

The size of the aperture of the 16 array Yagi antenna is $L = Md = 0.432$ m, and d is the length (=0.027 m) of the single Yagi antenna in the array direction. The Fraunhofer distance $d_f = 2L^2/\lambda = 128\lambda = 6.616$ m, which is the boundary of the far-field region. Therefore, the near-field region sampled in this simulation is close to the antenna at about $0.2d_f$, which is difficult to control accurately with the NFF approaches based on far-field AEP. Nevertheless, the following results in this paper show that it is sufficiently applicable when the proposed method is appropriately applied.

B. NAEP OF 16 × 1 QUASI-YAGI ARRAY ANTENNA FOR ADAPTIVE RESOLUTION GRID

Using (5), 16 NAEPs, which are re-radiated from the 16 ID models, can be easily obtained. In Fig. 3, the NAEP

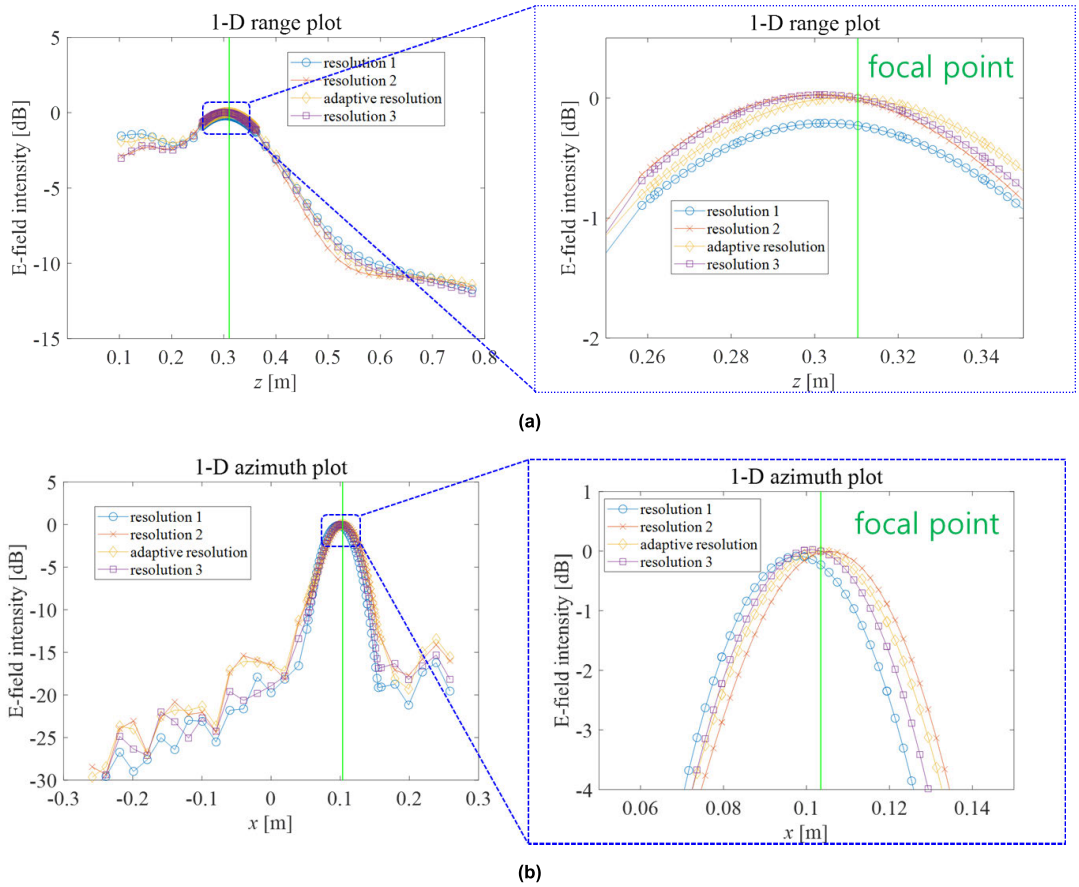

FIGURE 6. 1D NFF results for comparison of NFF results for 4 type grids shown in Fig. 4 (a) *x*-cut (range direction plot) (b) *z*-cut (azimuth direction plot).

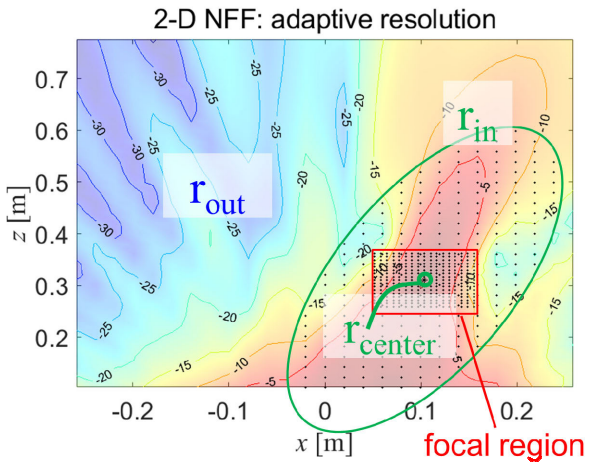

FIGURE 7. 2D NFF result using the adaptive resolution grid with graphical description for the focal point, ellipse radius of major and minor axes condition in table 1).

results for the adaptive resolution grid with ID models of port 4, 8 and 12 are shown as examples. The near-fields in the *xyz* range of [−0.2586 m∼0.2586 m, 0 m, and 0.1034 m∼0.6034 m] are calculated and used in the *x*, *y*, and *z* domains, respectively, when the center point of the antenna geometry is the origin, as shown in Fig. 2. The boresight direction of the array antenna is the +*z* direction, the antenna is arrayed along the *x*-axis and the near-field is sampled with respect to the *xz* plane. If the sampled near-field region includes the region close to the antenna in the radial direction, the performance of the near-field synthesis may deteriorate because the intensity of the near-field is absolutely large.

This region is difficult to control through the excitation coefficients. The near-field region should be sampled appropriately based on the radiation properties of the NFF antennas.

An adaptive resolution grid for NFF simulation is shown in steps 3 and 4 in Fig. 1. In Fig. 4, 4 types of near-field grid are shown and this is used to compare and verify the efficiency and accuracy of the adaptive resolution grid. For each resolution type, 16 NAEPs are required to be computed for each type of grid. In rows 2 to 4 of table 1, the comparison results of resolution, number of samples, and NAEP calculation times for 4 types of resolution grids are shown. The *resolution 1* to *resolution 3* consist of a uniform grid with different resolutions. The number of sampled points in the *resolution 3* case is similar to that of the adaptive resolution case. In the adaptive resolution grid, the entire region is first sparsely configured with *resolution 1*, and then finest *resolution 2* in the focal region is partially merged. In other words, the adaptive resolution grid is created with the right combination of high and low resolutions.

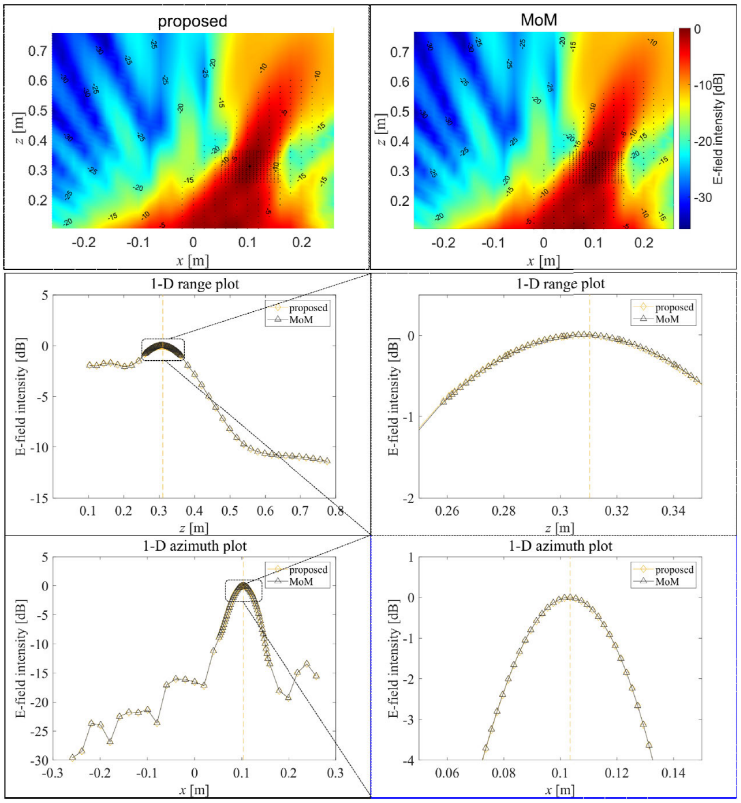

FIGURE 8. Comparative verification between the proposed method and MoM (FEKO) results (top) 2D NFF results using the proposed method and MoM (middle) 1D NFF results for *x*-cut (bottom) 1D NFF results for *z*-cut.

TABLE 1. Summary of NFF simulation results.

	resolution 1 (coarse)	*resolution 2* (finest)	*resolution 3* (medium)	*adaptive resolution*
parameters for (14)	focal point: [10.34 mm (2λ), 31.03 mm (6λ)] ellipse radius of major axes: 31.03 mm (6λ) ellipse radius of minor axes: 5.17 mm (λ) c_{center}: 0 dB, c_{out}: −4 dB			
resolution	20 mm	6.67 mm	17.2 mm	6.67 mm (focal region) 20 mm (other region)
num. of samples (N_x x N_z)	945 (27 x 35)	8058 (79 x 102)	1240 (31 x 40)	1234 (27 x 35 + 17 x 17)
NAEP calculation time	34.66 s	1968.3 s	47.23 s	36.5 s
CVX optimization time	31.0 s	624.3 s	51.1 s	51.7 s
focal shift (range)	-43.8 mm	-9.9 mm	-29.8 mm	-8 mm
focal shift (azimuth)	-13.9 mm	0 mm	-8 mm	-2 mm
DoF	89.8 mm	89.8 mm	89.8 mm	109.5 mm
FW	19.9 mm	27.9 mm	23.9 mm	25.9 mm
The NFF simulation results were computed by Intel(R) Core(TM) i7-10750H CPU@2.60GHz and RAM@16 GB.				

The x and y coordinates of the focal point were set to 10.34 mm (2λ) and 31.03 mm (6λ). The focal region was defined as a rectangle around the focal point. For comparison of results with *resolution 3*, the focal area was selected as the point where the number of samples equal to that of *resolution 3*.

C. NFF BASED ON CONVEX OPTIMIZATION OF 16 × 1 QUASI-YAGI ARRAY ANTENNA

First, we require to define the $\mathbf{r}_{in}$ and $\mathbf{r}_{out}$ regions to apply the convex optimization based on (14). As shown in Fig. 7, the center of the ellipse $\mathbf{r}_{in}$ can be defined as the focal point, and the ellipse radius of the major and minor axes are set as 31.03 mm (6λ) and 5.17 mm (λ), respectively.

In addition, in order to apply (14) for the Yagi array antenna, c_{center} and c_{out} were set to 0 dB and −4 dB, respectively. The amplitudes of electric field and corresponding weight coefficients are proportional each other. That is, not the absolute values of c_{center} and c_{out}, but the relative difference between c_{center} and c_{out} is meaningful. N_{iter} and δ are 3 and 0.01, respectively. These parameters should be determined appropriately that resulting solution sufficiently converges.

Each constraint must be properly adjusted to satisfy the conditions of the focal point, and $\mathbf{r}_{in}$, which are the designated specifications of the NFF antenna. The w_m^{AEP} can be obtained through the optimization process in (14), and the resulting near-field distribution of the array antenna is shown in Fig. 5 and Fig. 6 in the two-dimensional and one-dimensional way.

The two-dimensional plots of the near-field are on the same plane with the radiation antenna. The results seem almost same because of the applying optimizations with same constraints, but the source data are different. It is difficult to recognize the differences through the graphical results in Fig. 5, thus the numerical parameters and reformatting of the near-field profile are needed to analyze in terms of the NFF. Through the one-dimensional plots in range and azimuth direction based on the focal point, the resulting focal shifts can be determined.

With the results of Table 1 and Fig. 6, it can be seen that the accuracy of the adaptive resolution grid is similar to resolution 2, which has the finest resolution result. The indicator of accuracy is the focal shift, and a smaller focal shift means that the beam can be focused at a desired focal point. By applying the proposed adaptive resolution, the near-field can be focused at a desired point as accurate as when the near-field data set is extremely precisely extracted. However, the case of the finest resolution (resolution 2) needs much more larger computation time as shown in Table 1. The calculation time of the proposed approach is similar to the results of the resolution 3 because those two data sets have similar number of the near-field samples. The computation time during the NAEP calculation and solving the optimization is an indicator of the NFF efficiency, and these values are dominantly determined by the number of samples. In other words, it can be analyzed that NFF using the adaptive resolution grid has both high accuracy and high efficiency than NFF using the general uniform grids.

D. VALIDATION OF THE RESULTS BY COMPARISON WITH THE MOMENT METHOD

In order to verify the implementation reliability of the IDM-based NFF algorithm. For the same simulation case for NFF, two results were obtained to be compared with. The one is derived by the proposed IDM-based method, and the other one is derived by MoM (FEKO). The adaptive resolution is adopted to the simulations as described in Section IV. For the MoM simulation, the same beam coefficients optimized from the proposed NFF algorithm are applied to 16 Yagi array antenna. In Fig. 8, the resulting near-field derived by the proposed method and the MoM on the same plane and the same line represented in Fig. 4 and Fig. 5 are shown. By comparing the results, it can be validated that the near-field results from the proposed IDM based NFF algorithm is numerically reliable.

V. CONCLUSION

In this paper, the three issues of NFF mentioned above are clearly resolved through the proposed NFF technique. The problem of data acquisition of the near-field mentioned as the first problem was clearly solved in the form of using an IDM. Using the once acquired IDM, it is possible to obtain an accurate radiation field for any desired far-field or near-field observation area by re-radiation of the IDM current. The efficiency problem in applying the optimization method mentioned as the second problem was solved by introducing convex optimization and utilizing NAEP on the adaptive resolution grid. The adaptive resolution gird has a high resolution for the focal region and a low resolution for the other region. Moreover, through convex optimization, we were able to freely design the desired focus area and focus the near-field energy in the focus area. The antenna mutual coupling problem, mentioned as the third problem, was solved through AEP-IDM. The IDM that perfectly reflects the mutual coupling effect was extracted using far-field AEP, and the NAEP was generated by re-radiating the IDM to reflect the mutual coupling between antennas in the NFF problem.

The validation results of the proposed method were shown through the comparison of NFF results for 4 grid types. Compared to the finest resolution, the computation time of the adaptive resolution for the optimization is reduced to 8%. Nevertheless, it represents almost the same focal shift. It can be concluded that the focal shift is dominantly limited by the resolution in proximity to the focal point. The results were validated by the field values calculated with the MoM for the same radiation conditions.

The validations represented in this study were performed by only the simulation results. However, if the source data (far-field data in this study) was extracted by the measurements, there could be error in the NFF results according to the uncertainty of the field measurements and sensitivity of the antenna modeling. In more practical aspects and realistic manner, the proposed NFF approach can be assessed in the further works.

REFERENCES

[1] P. Nepa and A. Buffi, "Near-field-focused microwave antennas: Near-field shaping and implementation," *IEEE Antennas Propag. Mag.*, vol. 59, no. 3, pp. 42–53, Jun. 2017.
[2] D. Jeon, M.-S. Kim, S.-J. Ryu, D.-H. Lee, and J.-K. Kim, "Fully printed chipless RFID tags using dipole array structures with enhanced reading ranges," *J. Electromagn. Eng. Sci.*, vol. 17, no. 3, pp. 159–164, Jul. 2017.
[3] C. Y. Chang, H. T. Chou, Z. C. Tsai, M. Y. Lee, and C. T. Yu, "Beam steering technology of near-field focused phased array of antennas for RFID applications," in *Proc. Int. Symp. Antennas Propag. (ISAP)*, Busan, South Korea, Oct. 2018, pp. 1–3.
[4] H.-T. Chou, M.-Y. Lee, and C.-T. Yu, "Subsystem of phased array antennas with adaptive beam steering in the near-field RFID applications," *IEEE Antennas Wireless Propag. Lett.*, vol. 14, pp. 1746–1749, 2015.
[5] A. Buffi, A. A. Serra, P. Nepa, and G. Manara, "A focused planar microstrip array for 2.4 GHz RFID readers," *IEEE Trans. Antennas Propag.*, vol. 58, no. 5, pp. 1536–1544, May 2010.
[6] R. Siragusa and S. Tedjini, "Tunable near-field focused circular phase-array antenna for 5.8-GHz RFID applications," *IEEE Antennas Wireless Propag. Lett.*, vol. 10, pp. 33–36, 2011.
[7] H.-T. Chou, N.-N. Wang, H.-H. Chou, and J.-H. Qiu, "An effective synthesis of planar array antennas for producing near-field contoured patterns," *IEEE Trans. Antennas Propag.*, vol. 59, no. 9, pp. 3224–3233, Sep. 2011.
[8] A. Razavi, R. Maaskant, J. Yang, and M. Viberg, "Optimal aperture distribution for maximum power transfer in planar lossy multilayered matters," in *Proc. 9th Eur. Conf. Antennas Propag.*, Lisbon, Portugal, Apr. 2015, pp. 1–5.
[9] K. D. Stephan, J. B. Mead, D. M. Pozar, L. Wang, and J. A. Pearce, "A near field focused microstrip array for a radiometric temperature sensor," *IEEE Trans. Antennas Propag.*, vol. 55, no. 4, pp. 1199–1203, Apr. 2007.

[10] M. Bogosanovic and A. G. Williamson, "Microstrip antenna array with a beam focused in the near-field zone for application in noncontact microwave industrial inspection," *IEEE Trans. Instrum. Meas.*, vol. 56, no. 6, pp. 2186–2195, Dec. 2007.
[11] N. S. Karnik, R. Tulpule, M. Shah, P. S. Verma, C. Y. Huang, J. Y. Cha, A. Pandya, S. Usman, V. Pulipati, P. Pagadala, and B. P. Kumar, "Design, simulation and experimental study of near-field beam forming techniques using ormal waveguide arrays," *IET Microw., Antennas Propag.*, vol. 4, no. 2, pp. 162–174, 2010.
[12] A. Razavi, R. Maaskant, J. Yang, and M. Viberg, "Maximum aperture power transmission in lossy homogeneous matters," *IEEE Antennas Wireless Propag. Lett.*, vol. 14, pp. 175–178, 2015.
[13] J. T. Loane and S.-W. Lee, "Gain optimization of a near-field focusing array for hyperthermia applications," *IEEE Trans. Microw. Theory Techn.*, vol. 37, no. 10, pp. 1629–1635, Oct. 1989.
[14] X. He, W. Geyi, and S. Wang, "Optimal design of focused arrays for microwave-induced hyperthermia," *IET Microw., Antennas Propag.*, vol. 9, no. 14, pp. 1605–1611, Nov. 2015.
[15] R. Van der Linden and H. J. Visser, "Analysis, design and realization of a near-field focused RF power transfer system," *J. Phys. Conf. Ser.*, vol. 476, no. 1, pp. 1–5, Dec. 2013.
[16] S. Yu, H. Liu, and L. Li, "Design of near-field focused metasurface for high-efficient wireless power transfer with multifocus characteristics," *IEEE Trans. Ind. Electron.*, vol. 66, no. 5, pp. 3993–4002, May 2019.
[17] Z. Nie and Y. Yang, "A model independent scheme of adaptive focusing for wireless powering to in-body shifting medical device," *IEEE Trans. Antennas Propag.*, vol. 66, no. 3, pp. 1497–1506, Mar. 2018.
[18] G. V. Borgiotti, "Maximum power transfer between two planar apertures in the Fresnel zone," *IEEE Trans. Antennas Propag.*, vol. AP-14, no. 2, pp. 158–163, Mar. 1966.
[19] J. Álvarez, R. G. Ayestarán, and F. Las-Heras, "Optimization framework on antenna arrays for near field multifocusing," in *Proc. IEEE Antennas Propag. Soc. Int. Symp.*, Chicago, IL, USA, Aug. 2012, pp. 1–2.
[20] J. Álvarez, R. G. Ayestarán, G. León, L. F. Herrán, and A. Arboleya, "Near field multifocusing on antenna arrays via non-convex optimisation," *IET Microw., Antennas Propag.*, vol. 8, no. 10, pp. 754–764, Jul. 2014.
[21] R. C. Hansen, "Focal region characteristics of focused array antennas," *IEEE Trans. Antennas Propag.*, vol. AP-33, no. 12, pp. 1328–1337, Dec. 1985.
[22] A. Buffi, P. Nepa, and G. Manara, "Design criteria for near-field-focused planar arrays," *IEEE Antennas Propag. Mag.*, vol. 54, no. 1, pp. 40–50, Feb. 2012.
[23] M. S. Narasimhan and B. Philips, "Synthesis of near-field patterns of arrays," *IEEE Trans. Antennas Propag.*, vol. AP-35, no. 2, pp. 212–218, Feb. 1987.
[24] E. J. Candès and M. B. Wakin, "An introduction to compressive sampling," *IEEE Signal Process. Mag.*, vol. 25, no. 2, pp. 21–30, Mar. 2008.
[25] Z. X. Huang and Y. J. Cheng, "Near-field pattern synthesis for sparse focusing antenna arrays based on Bayesian compressive sensing and convex optimization," *IEEE Trans. Antennas Propag.*, vol. 66, no. 10, pp. 5249–5257, Oct. 2018.
[26] G. G. Bellizzi, D. A. M. Iero, L. Crocco, and T. Isernia, "Three-dimensional field intensity shaping: The scalar case," *IEEE Antennas Wireless Propag. Lett.*, vol. 17, no. 3, pp. 360–363, Mar. 2018.
[27] D. A. M. Iero, L. Crocco, and T. Isernia, "Constrained power focusing of vector fields: An innovative globally optimal strategy," *J. Electromagn. Waves Appl.*, vol. 29, pp. 1708–1719, Jul. 2015.
[28] S. M. Mikki and A. A. Ksihk, "Theory and applications of infinitesimal dipole models for computational electromagnetics," *IEEE Trans. Antennas Propag.*, vol. 54, no. 5, pp. 2764–2775, May 2007.
[29] T. S. Sijher and A. A. Kishk, "Antenna modeling by infinitesimal dipoles using genetic algorithms," *Prog. Electromagn. Res.*, vol. 52, pp. 225–254, 2005.
[30] S. Clauzier, S. M. Mikki, and Y. M. M. Antar, "Design of near-field synthesis arrays through global optimization," *IEEE Trans. Antennas Propag.*, vol. 63, no. 1, pp. 151–165, Jan. 2015.
[31] S. J. Yang, Y. D. Kim, D. J. Yun, D. W. Yi, and N. H. Myung, "Antenna modeling using sparse infinitesimal dipoles based on recursive convex optimization," *IEEE Antennas Wireless Propag. Lett.*, vol. 17, no. 4, pp. 662–665, Apr. 2018.
[32] Y.-D. Kim, S.-J. Yang, N.-H. Myung, and J.-W. Yu, "Improved prediction of the wideband beam pattern shape of antenna array based on infinitesimal dipole modeling," *IEEE Antennas Wireless Propag. Lett.*, vol. 17, no. 12, pp. 2309–2313, Dec. 2018.
[33] S. J. Yang, Y. D. Kim, H. W. Jo, and N. H. Myung, "Alternative method for obtaining antenna current green's function based on infinitesimal dipole modeling," *IEEE Trans. Antennas Propag.*, vol. 67, no. 4, pp. 2583–2590, Apr. 2019.
[34] S.-J. Yang, D.-J. Yun, H.-J. Kim, J.-I. Lee, W.-Y. Yang, and N.-H. Myung, "Antenna far-field prediction using restricted IDM based convex optimization," in *Proc. IEEE Asia Pacific Microw. Conf. (APMC)*, Nov. 2017, pp. 737–739.
[35] M. Serhir, P. Besnier, and M. Drissi, "Antenna modeling based on a multiple spherical wave expansion method: Application to an antenna array," *IEEE Trans. Antennas Propag.*, vol. 58, no. 1, pp. 51–58, Jan. 2010.
[36] S. Clauzier, S. M. Mikki, and Y. M. M. Antar, "A generalized methodology for obtaining antenna array surface current distributions with optimum cross-correlation performance for MIMO and spatial diversity applications," *IEEE Antennas Wireless Propag. Lett.*, vol. 14, pp. 1451–1454, 2015.
[37] J. F. Izquierdo, J. Rubio, J. Corcoles, and R. Gomez-Alcala, "Efficient radiation antenna modeling via orthogonal matching pursuit in terms of infinitesimal dipoles," *IEEE Antennas Wireless Propag. Lett.*, vol. 15, pp. 444–447, 2016.
[38] D. M. Pozar, "The active element pattern," *IEEE Trans. Antennas Propag.*, vol. 42, no. 8, pp. 1176–1178, Sep. 1994.
[39] P. J. Kajenski, "Phase only antenna pattern notching via a semidefinite programming relaxation," *IEEE Trans. Antennas Propag.*, vol. 60, no. 5, pp. 2562–2565, May 2012.
[40] Y. Liu, J. Bai, K. D. Xu, Z. Xu, and F. Han, "Linearly polarized shaped power pattern synthesis with sidelobe and cross-polarization control by using semidefinite relaxation," *IEEE Trans. Antennas Propag.*, vol. 66, no. 6, pp. 3207–3212, Jun. 2018.
[41] B. Fuchs, "Application of convex relaxation to array synthesis problems," *IEEE Trans. Antennas Propag.*, vol. 62, no. 2, pp. 634–640, Feb. 2014.
[42] S. E. Nai, W. Ser, Z. L. Yu, and H. Chen, "Beampattern synthesis for linear and planar arrays with antenna selection by convex optimization," *IEEE Trans. Antennas Propag.*, vol. 58, no. 12, pp. 3923–3930, Dec. 2010.
[43] M. Grant and S. P. Boyd. (Sep. 2013). *CVX: MATLAB Software for Disciplined Convex Programming, Version 2.0 Beta*. [Online]. Available: http://cvxr.com/cvx

SUNG JUN YANG was born in Ansan-si, South Korea, in 1992. He received the B.S. degree and the integrated M.S. and Ph.D. degree in electrical engineering from the Korea Advanced Institute of Science and Technology (KAIST), Daejeon, South Korea, in 2014 and 2019, respectively. After the graduation, he worked as a Postdoctoral Researcher with the RF Systems and Solutions Laboratory, KAIST. He is currently working as an Intern at the Foundation for Research on Information Technologies in Society (IT'IS), Zürich, Switzerland, and as a Postdoctoral Researcher at the Swiss Federal Institute of Technology (ETH), Zürich. His research interests include computational electromagnetics, antenna modeling, and electromagnetic exposure assessment.

YOUNG DAM KIM was born in Suwon, South Korea, in 1988. He received the B.S. degree in electronics engineering from Ajou University, Suwon, in 2011, and the M.S. and Ph.D. degrees in electrical engineering from the Korea Advanced Institute of Science and Technology (KAIST), Daejeon, South Korea, in 2013 and 2017, respectively. He worked as a Senior Engineer with Samsung Electronics Network Business, Suwon, in 2017. He worked as a Postdoctoral Researcher at the KAIST, in 2018. He worked as a Senior Researcher with Agency for Defense Development (ADD), South Korea, from 2019 to 2020. He is currently an Assistant Professor with the Department of Electronics Engineering, Chungnam National University (CNU), Daejeon. His current research interests include the analysis of active phased antenna array and electromagnetic scattering problems based on applied computational electromagnetics.